Ferguson et al., http://www.jcb.org/cgi/content/full/jcb.201604128/DC1

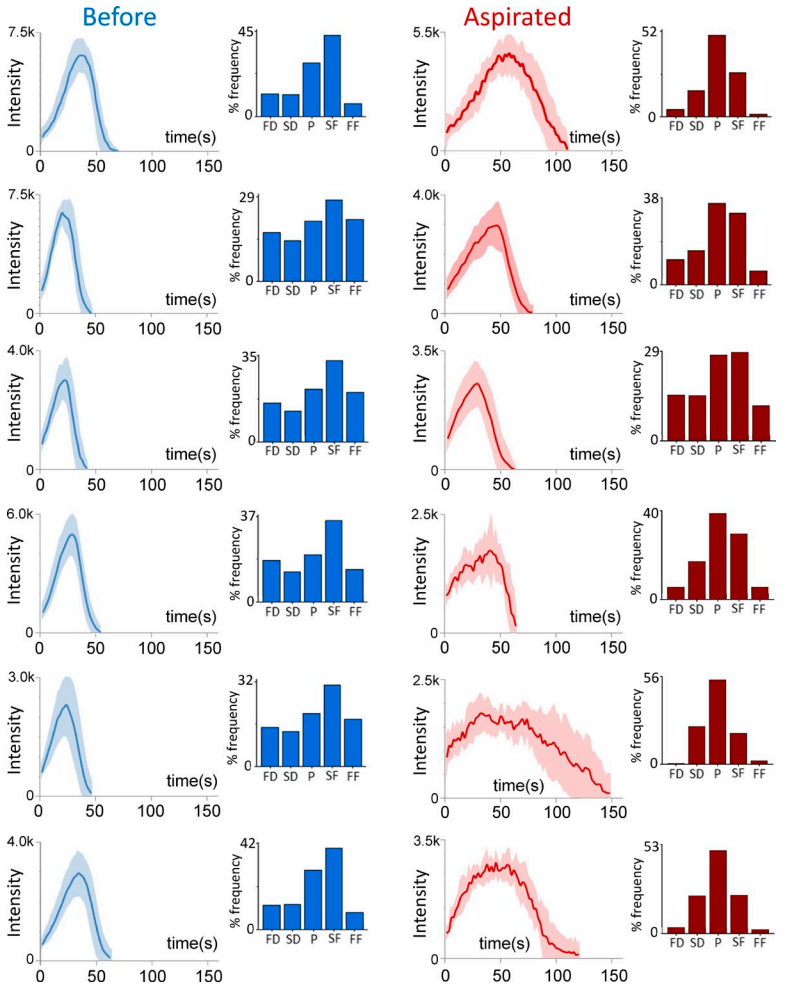

Figure S1. **Hierarchical clustering of CCS traces.** CCS trace clusters emerging before (blue) and during (red) micropipette aspiration are shown as mean ± standard deviation (shaded area). Growth rate histograms obtained using the traces in each cluster are shown next to the intensity profiles. FD, fast dissolution; FF, fast formation; P, plateau; SD, slow dissolution; SF, slow formation.

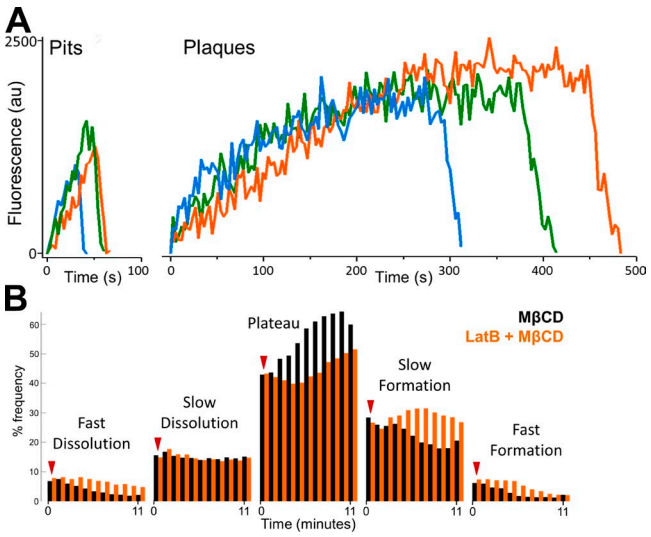

Figure S2. **CCS dynamics in cholesterol-depleted cells.** (A) Example intensity traces of clathrin-coated pits and plaques detected in a BSC1 cell before and after cholesterol depletion by MβCD treatment, respectively. (B) Percentage frequencies of the five growth phases are plotted as a function of time after addition of MβCD (4 mM final concentration; marked by the red arrowheads). Each bar in the histograms represents the frequency of CCS growth rates obtained from 1-min-long temporal windows. For each minute, growth rate histograms are calculated from a pool of CCS traces assembled from multiple cells (MβCD only: N_{cells} = 6 and N_{traces} = 23,667; latrunculin B [LatB] + MβCD: N_{cells} = 4 and N_{traces} = 37,911). Inhibition of CCS dynamics is less effective within cells that are pretreated with latrunculin B (2 µM final concentration; orange bars) 5 min before MβCD. Latrunculin B antagonizes the effect of MβCD by reducing the membrane–cytoskeleton adhesion energy (Hochmuth et al., 1996; Marcus and Hochmuth, 2002).

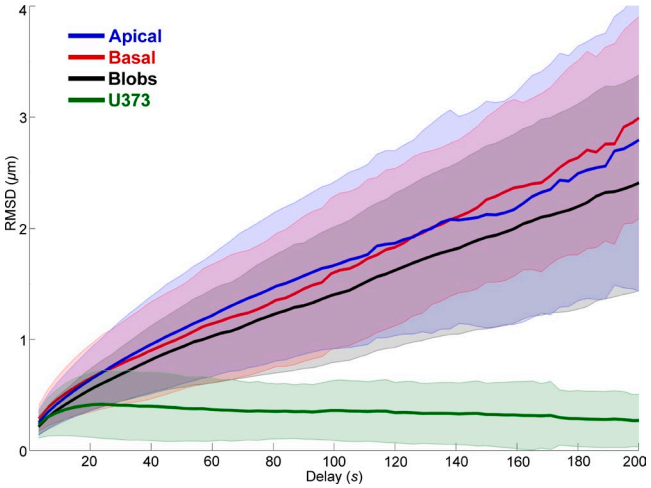

Figure S3. **CCS motility in cultured cells and *Drosophila* embryos.** Root mean square displacements (mean ± standard deviation) are measured at different lag times for CCS traces detected in *Drosophila* amnioserosa cells (N_{apical} = 16,279, N_{basal} = 8,714, and N_{blobs} = 1,407) and U373 cells transiently expressing CLC-mCherry (N_{cells} = 4 and N_{traces} = 23,630).

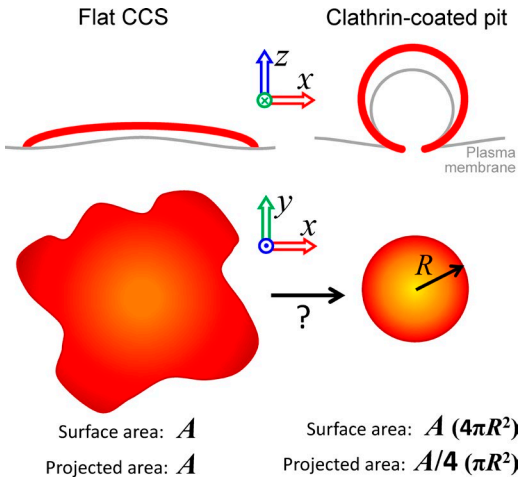

Figure S4. **Flat CCSs and clathrin-coated pits.** Surface area (A) of a flat CCS is equal to its projected area on the x–y plane. For a clathrin-coated pit, however, the surface area ($A = 4\pi R^2$, where R is the pit radius) is approximately fourfold greater than the projected area (πR^2). Therefore, transformation of a flat CCS into a pit requires a fourfold reduction in the projected area.

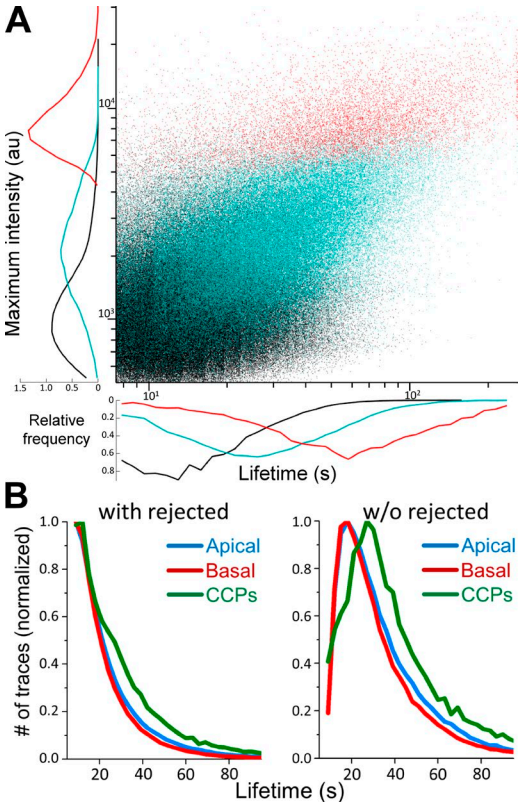

Figure S5. **Classification of CCS traces.** (A) Scatterplot shows lifetime (x axis) and maximum intensity (y axis) of CCS traces detected at *Drosophila* amnioserosa (N_{cells} = 38). We classified the traces into three categories (see Materials an methods): (1) Rejected (black spots, N_{traces} = 204,308). These traces that have very low signal to noise and their growth or dissolutions cannot be determined. Rejected traces are not used in calculation of growth rate distributions. (2) Blobs (red; N_{traces} = 8,805). These are very bright traces that are generally located at the perinuclear regions. (3) Bona fide endocytic carriers (cyan; N_{traces} = 115,253). Next to each axis are normalized histograms to help elucidate the density of points. Because lifetimes are in discrete frames, they have been spread with an even random distribution to make the figure intelligible. (B) A comparison of CCS lifetime distributions obtained from apical and basal amnioserosa with clathrin-coated pits (CCPs) detected in cultured BSC-1 cells stably expressing AP2-GFP. The distribution on the right omits the rejected traces, which have low signal to noise (Amnioserosa: $N_{embryos}$ = 2, N_{cells} = 75, N_{traces} = 329,871, and $N_{rejected}$ = 205,858; CCPs: N_{cells} = 3, N_{traces} = 32,743, and $N_{rejected}$ = 20,741).

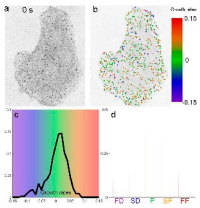

Video 1. **CCS growth rate distributions.** (A) Inverted image shows CCS activity at the ventral surface of a BSC-1 cell expressing AP2-GFP. (B) Each CCS in A is color-coded according to its instantaneous growth rate. (C) For each frame in the movie, distributions are assembled using the growth rates in B. (D) Growth rate distributions are shown as bar plots, where each bin represents a different growth phase (FD, fast dissolution; FF, fast formation; P, plateau; SD, slow dissolution; SF, slow formation).

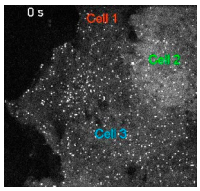

Video 2. **Impairment of CCS dynamics upon acute cholesterol depletion.** (top) Three BSC-1 cells expressing AP2-GFP. MβCD treatment is approximately t = 360 s. (middle) Growth rate histograms of the three cells generated from trace data acquired from 30-s-long temporal windows. (bottom) Temporal evolution of the predicted traces obtained using the analogy of growth rate distributions with the library clusters.

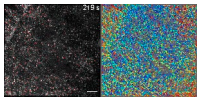

Video 3. **3D tracking of CCSs at *Drosophila* amnioserosa.** (left) Maximum z-projection of a 3D time-lapse movie acquired at the amnioserosa tissue of a late *Drosophila* embryo expressing CLC-GFP. Blobs are marked with red crosses. (right) CCS traces color-coded according to axial positions. Color map is the same with Fig. 8 B. Bar, 8 µm.

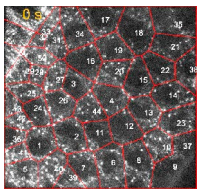

Video 4. **Determining cell boundaries by tracking amnioserosa nuclei.** Movie shows the dynamic Voronoi diagram used for determining amnioserosa cell boundaries at different time points. Positions of amnioserosa nuclei (shown with numbers) are used as a generating point of each Voronoi cell.

Provided online is the MATLAB-based software used for our analysis to be used or modified as fits the user's needs. The software zip file includes a README file, clearly commented code, and example data files.

References

Hochmuth, F.M., J.Y. Shao, J. Dai, and M.P. Sheetz. 1996. Deformation and flow of membrane into tethers extracted from neuronal growth cones. *Biophys. J.* 70:358–369. http://dx.doi.org/10.1016/S0006-3495(96)79577-2

Marcus, W.D., and R.M. Hochmuth. 2002. Experimental studies of membrane tethers formed from human neutrophils. *Ann. Biomed. Eng.* 30:1273–1280. http://dx.doi.org/10.1114/1.1528614